Acta Crystallographica Section B
Structural Science
ISSN 0108-7681

Structures of mono-unsaturated triacylglycerols. V. The β'_1-2, β'-3 and β_2-3 polymorphs of 1,3-dilauroyl-2-oleoylglycerol (LaOLa) from synchrotron and laboratory powder diffraction data

Jan B. van Mechelen,[a]* Kees Goubitz,[a] Mihaela Pop,[b] Rene Peschar[a] and Henk Schenk[a]

[a]University of Amsterdam, HIMS/FNWI/Kristallographie, Valckenierstraat 65, 1018 Xe Amsterdam, The Netherlands, and [b]Avantium Technologies, Zekeringstraat 29, 1014 BV Amsterdam, The Netherlands

Correspondence e-mail: j.b.vanvechelen@uva.nl

Received 6 August 2008
Accepted 30 September 2008

The crystal structures of the β'_1-2, the β'-3 and the β_2-3 polymorphs of 1,3-dilauroyl-2-oleoylglycerol have been solved from powder diffraction data. The packing of the β_2-3 polymorph is similar to that of other *cis* mono-unsaturated triacylglycerols. Both the β' polymorphs are crystallized in a novel type of packing in which one of the saturated lauroyl chains is packed side-by-side with part of the unsaturated oleoyl chain.

1. Introduction

Oils and fats from vegetable sources are major components in many food and personal care products. Both the production conditions and the final quality and characteristics of these consumer products, like melting behaviour, texture, spreadability, gloss and shelf life, are determined to a large extent by the precise crystalline phase present. The characteristics of the crystallites (morphology, size, melting point, stability) can be quite different for the principle polymorphic form(s) (α, β' and β). For example, in products such as butter, margarines, shortenings and creams the fat should be crystallized in a stable β' polymorph, to avoid the graininess of the larger β-type crystallites (Watanabe *et al.*, 1992). In chocolate, however, the β phase is required because a $\beta' \rightarrow \beta$ phase transition in a finished chocolate product reduces its quality (Beckett, 1999).

Fats and oils consist of a large variety of triacylglycerols (TAGs). To obtain the desired functional and physical properties of a lipid-containing product, in most instances the fatty acid composition and/or its positional distribution at the glycerol requires modification. Interesterification (chemically or enzymatically catalyzed) is a widely adopted technique to produce lipids with a specific TAG composition and desired physical characteristics, the so-called structured lipids (SLs; Xu, 2000). For nutritional and pharmaceutical applications, SLs with medium chain-length fatty acids (MCFA), varying from caprylic acid (8:0) to lauric acid (12:0), at the *sn*-1 and *sn*-3 positions and an unsaturated long-chain fatty acid (LCFA) at the *sn*-2 position have been investigated intensively (Miura *et al.*, 1999; Osborn & Akoh, 2002). The pancreatic lipase is active towards fatty acids in the *sn*-1,3 positions and the MCFA are hydrolysed faster than LCFA at these positions. Once absorbed in the intestines, the MCFA are carried to the liver and become a source of energy. Unsaturated LCFA are also hydrolyzed and end up in the adipose tissue. Thus, potentially these mono-unsaturated SLs are concentrated and rapidly available sources of calories and nutrients. To apply SLs in confectionary and other nutritional products, their polymorphic phase behaviour should be under control. In contrast to TAGs that contain solely LCFAs, the structural

characteristics and polymorphic behaviour of SLs have not been studied in great detail.

Whereas single-crystal diffraction of mono-unsaturated TAGs is not really feasible, because of a lack of good quality and sizable single crystals, we demonstrated recently that crystal structure determination using high-resolution laboratory or synchrotron X-ray powder diffraction (XRPD) data, combined with direct-space search techniques, poses an attractive alternative. With this approach crystal structures have been established of several triple chain-length-packed polymorphs (β_2-3 and β_1-3) of *cis*-mono-unsaturated TAGs and mixtures thereof in parts I and II (van Mechelen *et al.*, 2006*a*,*b*), as well as double chain-length-packed polymorphs (β'_1-2, β-2) of *trans*-mono-unsaturated TAGs and related fully saturated TAGs in parts III and IV (van Mechelen *et al.*, 2008*a*,*b*).

In this paper we present the crystal structures of two metastable β' polymorphs (β'_1-2 and β'-3) and the stable β_2-3 polymorph of the structured *cis*-mono-unsaturated TAG 1,3-dilauroyl-2-oleoylglycerol (LaOLa), to our knowledge the first of this type for which now both β' and β models are available. In addition, it will be shown that the transition of α to β'_1-2 proceeds *via* a β'-2-like interim phase with low crystallinity.

This polymorph analysis and the structural models are expected to be useful in the future analysis and control of the $\beta' \rightarrow \beta_2$ phase transition of other *cis*-mono-unsaturated TAGs.

2. Materials and methods

2.1. Samples, sample preparation and data collection

LaOLa (colourless liquid at room temperature) was obtained from Unilever Research Laboratory (Vlaardingen, The Netherlands). For the preparation of samples glass capillaries (β'_1-2, β_2-3: Φ = 1.5 mm; β'-3: Φ = 1.0 mm) were filled at room temperature with liquid LaOLa. The β'_1-2 polymorph was grown on the BM16 diffractometer by cooling the capillary to $\sim$ 263 K and subsequently heating it to 273 K to increase the β'_1-2 crystallite size. Laboratory experiments have shown that the β'_1-2 polymorph crystallizes immediately at 263 K, and at the time resolution used (1 min) no preceding α or β'_2-2 polymorph has been observed. After completion of the crystallization of the β'_1-2 polymorph, the sample was cooled to 243 K and data were collected.

The β_2-3 polymorph of LaOLa was obtained by increasing the temperature of the β'_1-2 polymorph to 283 K and keeping it at this temperature until the conversion to the β_2-3 polymorph was completed. Afterwards, the β_2-3 sample was cooled and stored in dry ice until data collection.

The β'-3 polymorph was crystallized *in situ* on an X'pert Pro MPD diffractometer (PANalytical, Almelo, The Netherlands) equipped with a sealed Cu X-ray tube, an elliptical mirror, 0.01 rad Soller slits and an X'Celerator strip detector. Temperature was controlled with an Oxford Instruments Cryostream Compact (Oxford Instruments, Abingdon, England). A glass capillary with the β_2-3 polymorph of LaOLa was heated carefully just until the complete disappearance of the (002) and (004) reflections of the β_2-3 polymorph, subsequently cooled down to 282 K and after crystallization of the β'-3 polymorph was completed (1 h) XRPD data were collected.

Data for both β'_1-2 and β_2-3 LaOLa were collected at 243 K at the synchrotron beamline BM16 at the European Synchrotron Radiation Facility (ERSF, Grenoble, France). An Oxford Instruments Cryostream (Oxford Instruments, Abingdon, England) was used to control heating and cooling rates and data-collection temperature at BM16. The capillaries were mounted horizontally with the temperature-controlled N_2 stream flowing parallel to the length of the capillary.

All the glass capillaries were rotated during data collection. Continuous scans were made that were binned eventually in steps of 0.0025°2θ for β'_1-2, 0.008°2θ for β'-3 and 0.005°2θ for β_2-3.

The melting points T_m of the polymorphs have been determined on the PANalytical X'pert Pro MPD diffractometer by using a heating rate of 0.5 K min^{-1} and simultaneously monitoring the (changes between) XRPD patterns with 1 min scans from 0.7–25°2θ and a step size of 0.016°2θ.

Phase transitions were also analyzed with DSC using a Linkam DSC600 (Linkam Scientific Instruments Ltd, Tadworth, England). The liquid sample was quenched from 295 to 223 K with 60 K min^{-1} and subsequently heated at 6 K min^{-1}.

2.2. Indexing, model building, structure determination and refinement

Auto-indexing techniques, such as *ITO*, *TREOR* and *DICVOL* (for more programs see *e.g.* CCP14; Collaborative Computational Project, 1994) can be quite successful in indexing XRPD patterns, but not when applied to TAGs. In all XRPD patterns of TAGs that have been indexed to date, the low-angle region is dominated by a single reciprocal lattice zone (0*k*0) that is caused by a long (*b*) axis (> 40 Å) and the top half of low-angle peaks that is commonly used for indexing by auto-indexing techniques lacks non-zero indices related to the shortest axis. To have a better control of the indexing process, we developed our own indexing technique called

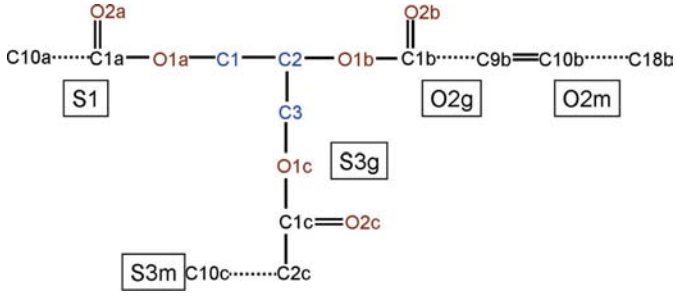

Figure 1
Chemical structure diagram and atomic numbering of LaOLa (g = glycerol side; m = methyl side). Partial (rigid body) acyl chains (see text) are defined as S1 (C2*a*–C10*a*), S3m (C2*c*–C10*c*), O2g (C2*b*–C9*b*) and O2m (C10*b*–C18*b*). S3g is C3–C2*c*.

Table 1
Long and short spacings, temperatures of X-ray data collection (T_{data}) and melting temperatures (T_m) of LaOLa polymorphs measured on the X'pert Pro MPD diffractometer.

The intensities of short spacings are marked as strong (s), medium (m) or weak (w).

Polymorph	α	β'_2-2	β'_1-2	β'-3	β_2-3
T_{data} (K)	248	248	248	282	284
T_m (K)	255	261†	287.5	286	290.5
Long spacing (Å)	40.9	40.8	36.6	55.1	52.6
Short spacings (Å)	4.12 (m)	4.18 (m)	4.48 (m)	4.47 (m)	4.58 (s)
		3.80 (w)	4.34 (m)	4.43 (s)	4.06 (m)
			4.26 (s)	4.36 (m)	3.92 (m)
			4.14 (s)	4.27 (s)	3.78 (m)
			3.87 (s)	4.24 (s)	3.70 (m)
			3.81 (m)	4.16 (s)	
			3.76 (w)	4.05 (m)	
				4.00 (s)	
				3.86 (s)	
				3.83 (s)	

† Phase transition temperature β'_2-2 → β'_1-2.

LSQDETC with which the unit cells of both β'_1-2 LaOLa and β_2-3 LaOLa have been determined. *LSQDETC* that runs in the *POWSIM* suite of programs (Peschar *et al.*, 2002) is based on a systematic ('brute force') cell-parameter search algorithm that operates in direct space, in contrast to the above-mentioned auto-indexing techniques. β'-3 LaOLa was indexed with the program *McMaille* (Le Bail, 2004) in Monte Carlo mode with search-space limitations.

For structure solution, starting models of the molecules were built in the *Z*-matrix form on the basis of the published structure of β_2-SOS (van Mechelen *et al.*, 2006*b*). To obtain an initial model, the program *FOX* was used in parallel tempering mode (Favre-Nicolin & Černý, 2002). Four (partial) acyl chains were handled as rigid bodies, the saturated lauroyl chains S1 (C2*a*–C10*a*) and S3m (*C*2*c*–C10*c*), and the two parts of the oleoyl chain denoted by O2g (C2*b*–C9*b*) and O2m (C10*b*–C18*b*), that are connected by the *cis* double bond (Fig. 1). The only degrees of freedom allowed in finding the molecular conformation were 11 torsion angles at the glycerol and the torsion angles on the two sides of the *cis* double bond. Initially, structural models without H atoms were used. During the structure-solution process, the torsion-angle restraints were relaxed one by one and eventually the most probable conformation of the molecules became clear. In the final stage of the structure solution the H atoms were added because their influence could not be neglected.

For the structure refinement the program *GSAS* (Larson & Von Dreele, 1987) was used. The background was fitted with a Chebyshev polynomial. To fit the profiles, *GSAS* function 4 was used for β_2-3 as well as for β'_1-2 and β'-3. This enabled a good fit of low-angle asymmetry as well as *hkl*-dependent broadening. To stabilize the refinement process, soft restraints were used for all bond angles and bond distances. Mean values for the restraints were taken from the Cambridge Structural Database (CSD; Allen, 2002). Soft planar constraints were applied to all four zigzag acyl chains S1, S3m, O2g and O2m defined above as well as to the three C═O groups with two adjacent C atoms. In the final stage of the refinement the preferred orientation (PO) was refined (March–Dollase) along the long axis of the unit cell. Only for β'_1-2 did this improve the *R* values (PO direction [010], ratio 1.04, range −1.7 to 4.7). The PO may have been induced by orientation of crystals along the wall of the capillary during their growth.

For the analysis of the structures two geometrical parameters were calculated for the four zigzag acyl chains defined above, the chain direction and the chain plane, which are the least-squares line and the least-squares plane through a set of atoms, respectively.

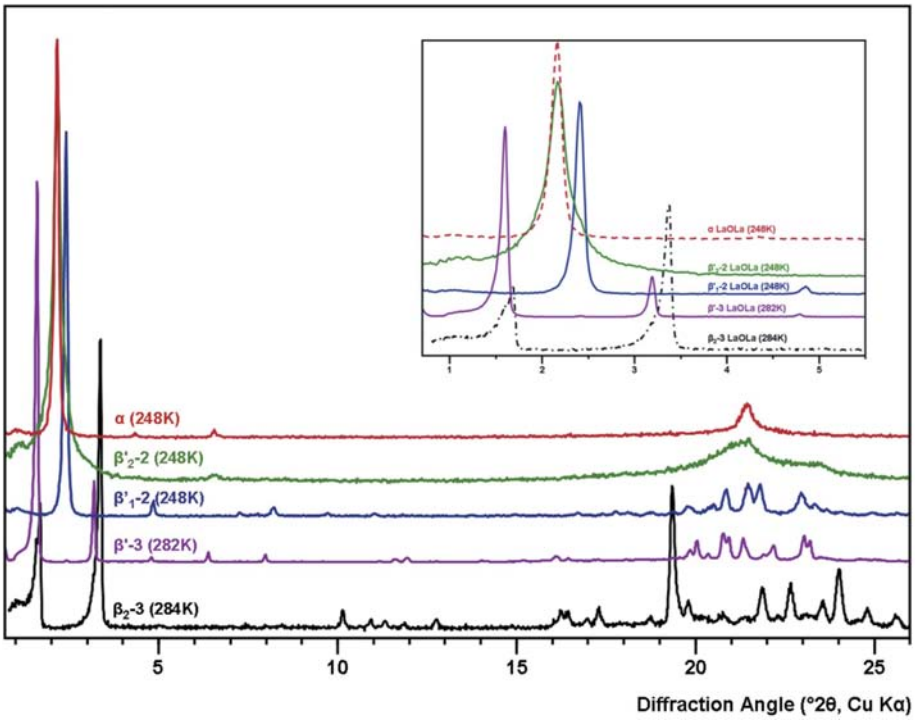

Figure 2
XPRD patterns of LaOLa polymorphs measured on the X'pert Pro MPD diffractometer.

3. Results and discussion

3.1. Polymorphs and their transitions

For LaOLa five different polymorphs (α, β'_2-2, β'_1-2, β'-3 and β_2-3) have been identified thus far. Their diffraction patterns measured on the X'pert Pro MPD diffractometer are

Table 2
Experimental details for the β'_1-2, β'-3 and β_2-3 polymorphs of LaOLa.

	β'_1-2 LaOLa	β'-3 LaOLa	β_2-3 LaOLa
Chemical formula	$C_{45}H_{84}O_6$	$C_{45}H_{84}O_6$	$C_{45}H_{84}O_6$
M_r	721.2	721.2	721.2
Cell setting, space group	Triclinic, $P\bar{1}$	Triclinic, $P\bar{1}$	Monoclinic, Cc
T_{data} (K)	243	282	243
a, b, c (Å)	12.05 (15), 36.59 (2), 5.427 (2)	5.450 (2), 7.736 (4), 56.10 (2)	5.449 (1), 104.42 (3), 8.143 (2)
α, β, γ (°)	95.0 (4), 101.5 (3), 84.6 (6)	81.5 (2), 89.7 (2), 90.2 (6)	90.0, 88.5 (2), 90.0
V (Å^3)	2328.9 (3)	2360.3 (3)	4631.6 (2)
Z	2	2	4
D_x (Mg m^{-3})	1.028	1.015	1.034
Radiation type	Synchrotron	Cu $K\alpha$	Synchrotron
Specimen form, colour	Cylinder: solid fat, white	Cylinder: solid fat, white	Cylinder: solid fat, white
Specimen size (mm)	20 × 1.5 × 1.5	12 × 1.0 × 1.0	20 × 1.5 × 1.5
Diffractometer	BM16 (ESRF)	X'Pert Pro MPD	BM16 (ESRF)
2θ range (°)	0.15–34	0.68–39.98	0.5–51
R factors and goodness-of-fit	R_p = 0.104, R_{wp} = 0.142, S = 2.26	R_p = 0.058, R_{wp} = 0.084, S = 4.30	R_p = 0.066, R_{wp} = 0.090, S = 2.49
Wavelength (Å)	0.4093	1.5418	0.85005
No. of parameters	467	451	416
$(\Delta/\sigma)_{max}$	0.27	0.44	0.42

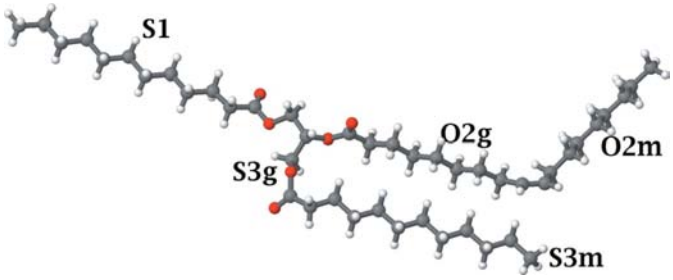

Figure 3
Molecular conformation of β'_1-2 LaOLa (g = glycerol side; m = methyl side) (http://submission.iucr.org/jtkt/serve/z/jL1yE8gu52XYaKT5/zz0000/0/).

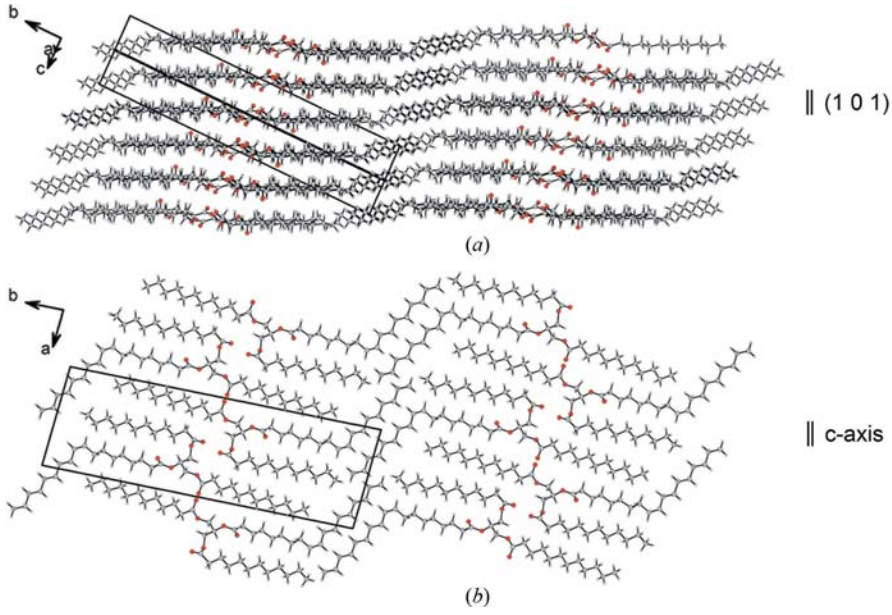

Figure 4
Crystal packing views of β'_1-2 LaOLa, (*a*) parallel to the (101) plane and (*b*) parallel to the *c* axis.

shown in Fig. 2, whereas long spacings, fingerprint lines (~ 3–5 Å, 19–25 °2θ, Cu $K\alpha$) and melting and phase transition points are listed in Table 1. A triple chain length γ polymorph that has been reported for other symmetric Sat-O-Sat type TAGs with longer saturated chains like POP and SOS (Sato *et al.*, 1989) has not been observed for LaOLa.

To obtain a pure α polymorph liquid LaOLa has to be quenched at at least 60 K min^{-1} to 250 K because lower cooling rates result in the formation of β'_1-2 prior to the start of the growth of α. The α polymorph has a double chain-length packing, a type of packing commonly found for the α polymorph of Sat-O-Sat′-type TAGs (Sato, 1996).

Starting from a pure α polymorph, the heating part of the DSC trace showed first a melting peak, followed by two crystallization peaks, the second appearing half a minute after the first, and finally ending with another melting peak. This DSC can be interpreted as the melting of the α polymorph, subsequently crystallization of an unstable (β') polymorph, the fast change of this unstable polymorph into a higher-melting form and finally the melting of this last (β') form. To identify the short-lived unstable phase, a temperature-controlled XRPD experiment has been carried out on the X'pert Pro MPD diffractometer. A capillary with the α polymorph was heated from 223 to 257 K and after a hold of 1 min cooled to 248 K to freeze the polymorph. In spite of having a long spacing close to that of the α phase, the novel polymorph

already has some β' characteristic features in the fingerprint area so it will be named β'_2-2, and the higher-melting one into which it changes β'_1-2 (Fig. 2, Table 1).

Because both the α and the β'_2-2 polymorphs have a double chain-length packing with equal long spacings, the melt does not seem to involve a change in chain-length packing. The long spacing diffraction peak of the β'_2-2 polymorph is broader than that of the other polymorphs (Fig. 2, insert). This can be indicative of a range of long spacings due to a more loose packing in the chain-length direction or of the presence of smaller crystallites. Both situations reflect an imperfect crystalline packing, as is also visible in the very broad fingerprint lines (Fig. 2).

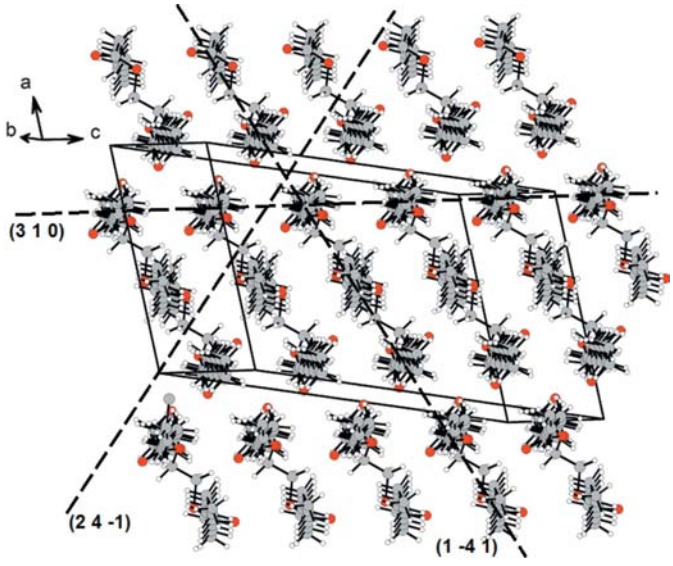

Figure 5
Crystal packing of β'_1-2 LaOLa viewed with the chain direction perpendicular to the paper. The orientation of lattice planes corresponding to strong reflections in the fingerprint area have been marked. For clarity, the O2m chain has been omitted.

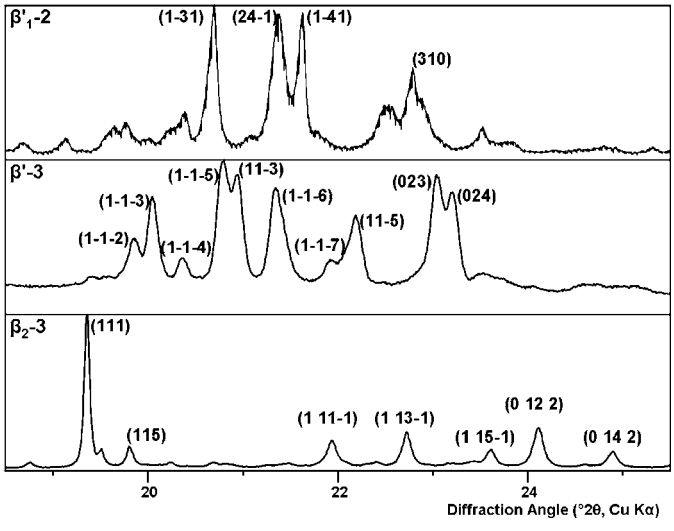

Figure 6
Fingerprint area of β'_1-2, β'-3 and β_2-3 rescaled to Cu $K\alpha$ radiation. The Miller indices of the strong reflections show the dominant zones.

Around its formation temperature (259 K) β'_2-2 is unstable, and when it is not frozen rapidly by decreasing the temperature it transforms directly into the β'_1-2 polymorph. The absence of a β'_2-2 melting endotherm in the DSC and the shorter β'_1-2 long spacing suggests that the β'_2-2 $\rightarrow$ β'_1-2 transition involves a reordering of the chains that leads to a more regular packing in the chain-length direction. The β'_1-2 polymorph is also preferred when starting from the fluid: except for high cooling rates (> 60 K min^{-1}) it rapidly crystallizes from the fluid and at 263 K the crystallization is completed within a few minutes. The instability of the β'_2-2 compared with the more stable β'_1-2 as well as the resemblance in the 2θ position of the sharp β'_1-2 fingerprint lines compared with the enveloping β'_2-2 diffraction maxima are similar to that observed for monoacid saturated TAGs (*e.g.* Kellens *et al.*, 1990) and *trans*-mono-unsaturated and related mixed-acid saturated TAGs (van Mechelen *et al.*, 2008*b*).

The β'-3 polymorph has a lower T_m (286 K) than that of the β'_1-2 polymorph (287.5 K). At 286 K β'-3 is less stable but below 286 K it is more stable than the β'_1-2 polymorph, as was revealed by a time- and temperature-solved XRPD experiment. When the β'-3 polymorph was heated with 0.1 K min^{-1} from 250 to 286 K, part of the β'-3 melted and another part transformed into β'_1-2. When the temperature of this partly molten mixture of β'-3 and β'_1-2 was decreased to 283 K, the molten fraction preferentially recrystallized to β'-3 and hardly at all to β'_1-2.

The observation of both double and triple chain-length-packed β' polymorphs for the same Sat-O-Sat′ TAG is not common. SOS has been reported to have a β'-3 polymorph and POP to have two β'-2 polymorphs (Sato *et al.*, 1989). Just like LaOLa, with β'-3 melting below the β'_1-2, POP and POS also have a triple chain-length polymorph (both denoted δ-3) that can be transformed into the higher melting β'_1-2 (Sato *et al.*, 1989; Arishima *et al.*, 1991).

The only way β_2-3 has been obtained until now is by conversion from β'_1-2 above 283 K. The β'_1-2 $\rightarrow$ β_2-3 transition is a slow process, as can be understood from their packing (see §3.5).

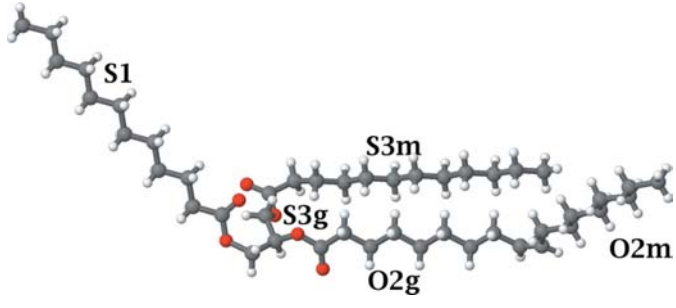

Figure 7
Molecular conformation of β'-3 LaOLa (g = glycerol side; m = methyl side). The S1 chain is pointing backwards and O2m is pointing forward out of the plane of the paper (http://submission.iucr.org/jtkt/serve/z/vT13nSGZj6h1xKNa/zz0000/0/).

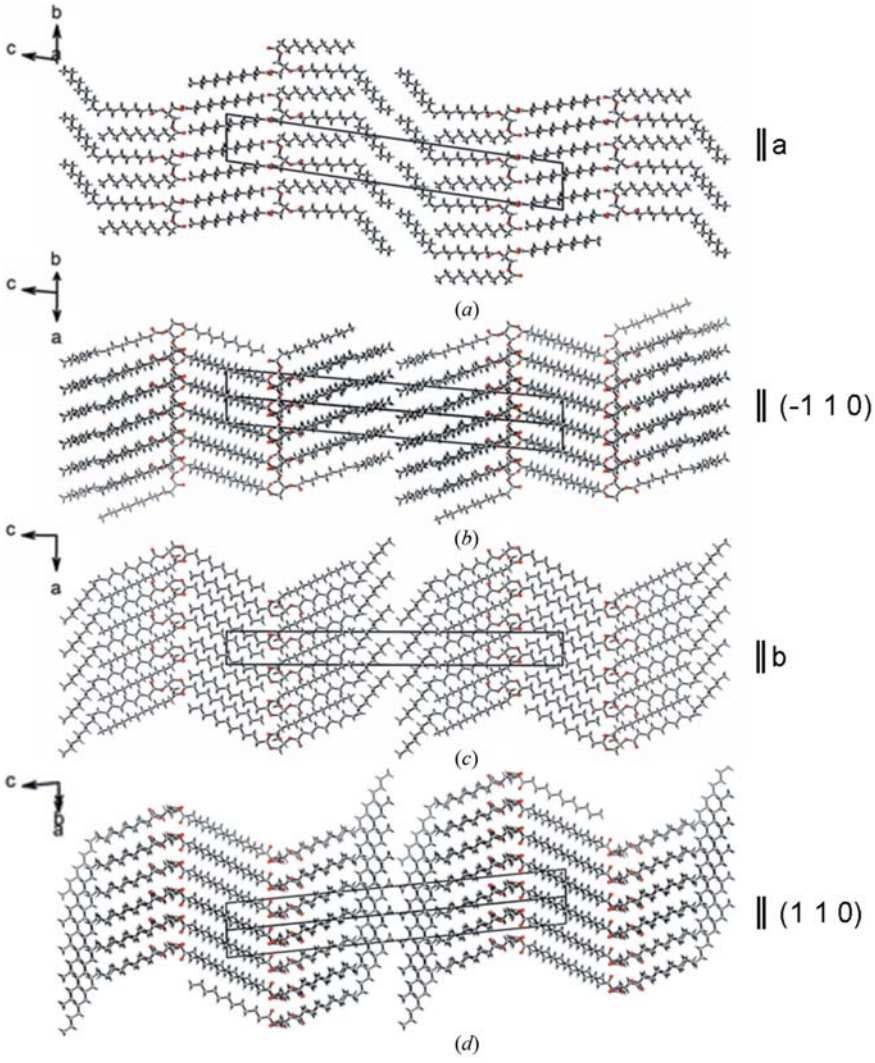

Figure 8
Parallel-packed chain layer views of the structure of β'-3 LaOLa when rotated around the normal to the *ab* plane: (*a*) parallel to the *a* axis; (*b*) parallel to the $(\bar{1}10)$ plane; (*c*) parallel to the *b* axis; (*d*) parallel to the (110) axis.

Whether an isothermal transition from pure β'-3 to β_2-3 is possible is not yet known. In the limited number of β'-3 $\rightarrow$ β_2-3 experiments that have been carried out so far β_2-3 seeds were present and simple annealing a mixture of β'-3 and β_2-3 close to the melting point of β'-3 led to conversion of β'-3 to β_2-3. Also in β'_2-2 with a small amount of β'-3 the conversion to β_2-3 seems to be blocked or at least very difficult to realise.

3.2. Structure of β'_1-2 LaOLa

The powder pattern of β'_1-2 LaOLa was indexed as triclinic and the structure was solved in the space group $P\bar{1}$ with a single molecule in the asymmetric unit. Experimental details for the structure are listed in Table 2. The observed and calculated diffraction pattern and a difference trace after structure refinement are given in the supplementary material (Fig. 13).[1]

In the literature on *cis*-mono-unsaturated TAG structures with saturated fatty acids at the *sn*-1,3 positions (Sat-O-Sat′), it is commonly assumed that in the β', β_2 and β_1 polymorphs the two saturated chains pack parallel to each other, while the O chain points in the opposite direction (Larsson, 1972; de Jong *et al.*, 1991; Sato & Ueno, 2001). This characteristic has indeed been found in the crystal structures of the β_2-3 and β_1-3 polymorphs of this type of TAG (van Mechelen *et al.*, 2006*a*,*b*).

Surprisingly, the crystal structure of β'_1-2 LaOLa, and also that of β'-3 LaOLa as discussed below, has a completely different type of packing, in which the S3m and O2g acyl chains are packed side-by-side and the S1 chain points in the opposite direction (Fig. 3). To show that the β'_1-2 LaOLa diffraction data cannot be explained by a model in which the S1 and S3m chains are packed side-by-side, several attempts have been made to solve the structure of the β'_1-2 polymorph (and that of β'-3), while enforcing the S1 and S3m chains to remain side-by-side. These attempts were not successful and it was observed that relaxation of the torsion-angle restraint in the S3g chain (C3—C2*c* in Fig. 1) invariably led to a swap of the S3m chain to being side-by-side with the O2g chain.

The molecules in the β'_1-2 polymorph (Fig. 3) are in a so-called chair conformation and almost flat, with the directions of the individual chains being positioned roughly in the same plane and with only the O2m chain direction being slightly rotated out of the plane defined by the other chain directions. In the refined structural model the zigzag planes of the O2m and O2g chains are slightly inclined with respect to the normal of the plane of the molecule, whereas the zigzag planes of the saturated chains are slightly inclined to the plane itself. Unfortunately, drawing conclusions from these zigzag orientations is not feasible because the limitation in resolution of the XRPD data does not allow determining a precise orientation of the zigzag planes. This situation is the same as for the

[1] Supplementary data for this paper are available from the IUCr electronic archives (Reference: DR5021). Services for accessing these data are described at the back of the journal.

β'_1-2 and β polymorphs of other mono-unsaturated TAGs (van Mechelen *et al.*, 2006*a*,*b*, 2008*a*,*b*).

In β'_1-2 the molecular flat 'chairs' are related pairwise by inversion centers and they are packed in layers (Fig. 4*a*) with the seats of the chairs facing each other, thus resulting in a double chain-length packing (Fig. 4*b*). Related by centers of symmetry, the O2m chains of neighboring pairs of molecules are parallel and form unsaturated zones within the layers of entangled molecules, although these zones are much smaller than in the β'-3 and β_2-3 polymorphs (see below).

In contrast to many other TAG packings, in β'_1-2 LaOLa no methyl end-plane can be discerned (Fig. 4*b*). When the structure is viewed parallel to the saturated chain direction (Fig. 5) it becomes clear that the strong β' characteristic diffraction maxima in the fingerprint area of the diffraction pattern (Fig. 6, upper pattern) are related to the packing of the columns of electron density formed by the chains.

3.3. Structure of β'-3 LaOLa

Like β'_1-2 LaOLa, the powder pattern of β'-3 LaOLa was indexed as triclinic and its structure solved in the space group $P\bar{1}$ with a single molecule in the asymmetric unit. Experimental details for the structure are listed in Table 2. The observed and calculated diffraction patterns and a difference trace after structure refinement are given in the supplementary material (Fig. 14).

As in β'_1-2, the S3m and O2g acyl chains are packed side-by-side and the S1 chain points in the opposite direction. However, the chair conformation of the molecules in β'-3 is not flat: the S1 chain is inclined to the plane through the O2m and O2g chains. (Fig. 7).

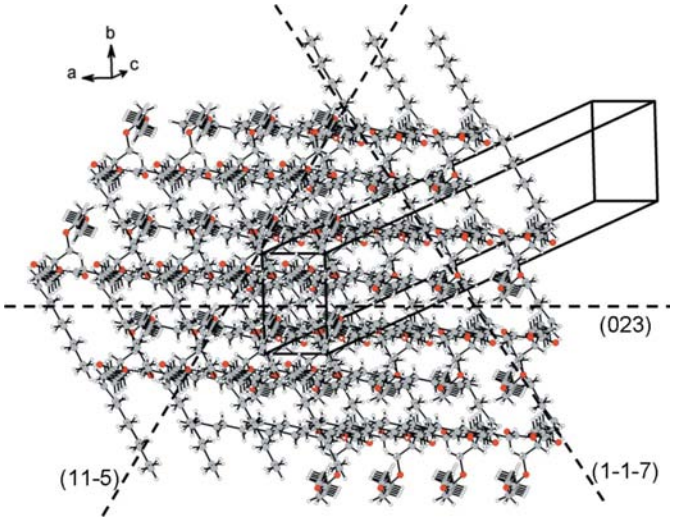

Figure 9
Crystal packing of β'-3 LaOLa viewed with the chain direction of the S3m and O2g chains perpendicular to the paper. The orientation of lattice planes corresponding to several strong reflections in the fingerprint area have been marked. For clarity, the unit-cell content between $z = 0.5$ and 1 has been omitted.

The molecular 'chairs' of the β'-3 polymorph are related pair-wise by inversion centers and result in a novel type of layered packing of the acyl chains that becomes visible when the structure is rotated around the normal to the *ab* plane. Fig. 8 shows four layer orientations from which three chain zones can be discerned. Pairs of S1 chains from opposing chairs form a zone around $z = 0$. The O2m chains are positioned in a second zone in the centre of the unit cell on both sides of the methyl end-plane at $z = 0.5$. The S3m and O2g chains form a third zone that is sandwiched between the S1 and the O2m zones. The methyl end-plane is smooth and the O2m chains on both sides of the methyl end-plane are not aligned (Fig. 8*b*). In a view parallel to the chair legs (S3m and O2g chains; Fig. 9) the relation between the dominant zones in the fingerprint area (Fig. 6, middle) and the columns of electron density of the chains is explained.

3.4. Structure of β_2-3 LaOLa

The crystal structure of β_2-3 LaOLa can be considered as another member of the set of β_2-3 type crystallized Sat-O-Sat′ TAGs, like POP, POS, SOS and mixtures thereof such as cocoa butter (van Mechelen *et al.*, 2006*b*) because of the similarity in the space group (*Cc*), molecular conformation and crystal packing. Experimental details for the structure are listed in Table 2. The observed and calculated diffraction patterns and a difference trace after structure refinement are given in the supplementary material (Fig. 15).

In the β_2-3 polymorph the saturated chains of each TAG molecule are packed side-by-side and the O chain points in the opposite direction (Fig. 10), a characteristic of the β_2-3 as well as the β_1-3 polymorphs of Sat-O-Sat′-type TAGs, and this results in a flat molecular chair conformation with all (partial) chain directions lying in the same plane. The flat molecular 'chairs' are related pairwise by glide planes and together with the *C* centering this leads to a packing that consists of two triple chain-length-packed zones (hereafter abbreviated as three-packs; Fig. 11). The two identical three-packs are related by translational symmetry, while inside a three-pack the molecules are related by glide-plane symmetry. The O chains form an unsaturated zone in the middle of the three-packs.

The packing of β_2-3 LaOLa has a terrace-type methyl end-plane that is best visible in a view parallel to the *a* axis (Fig. 11*c*). At the methyl end-plane the stacks of three-packs are not aligned (Fig. 11*d*). Rotation of the structure around the longest axis shows four orientations with ordered layers of acyl

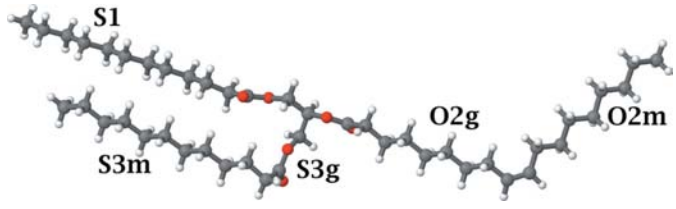

Figure 10
Molecular conformation of β_2-3 LaOLa (g = glycerol side; m = methyl side) (http://submission.iucr.org/jtkt/serve/z/mkyg6NB2gxymZp3H/zz0000/0/).

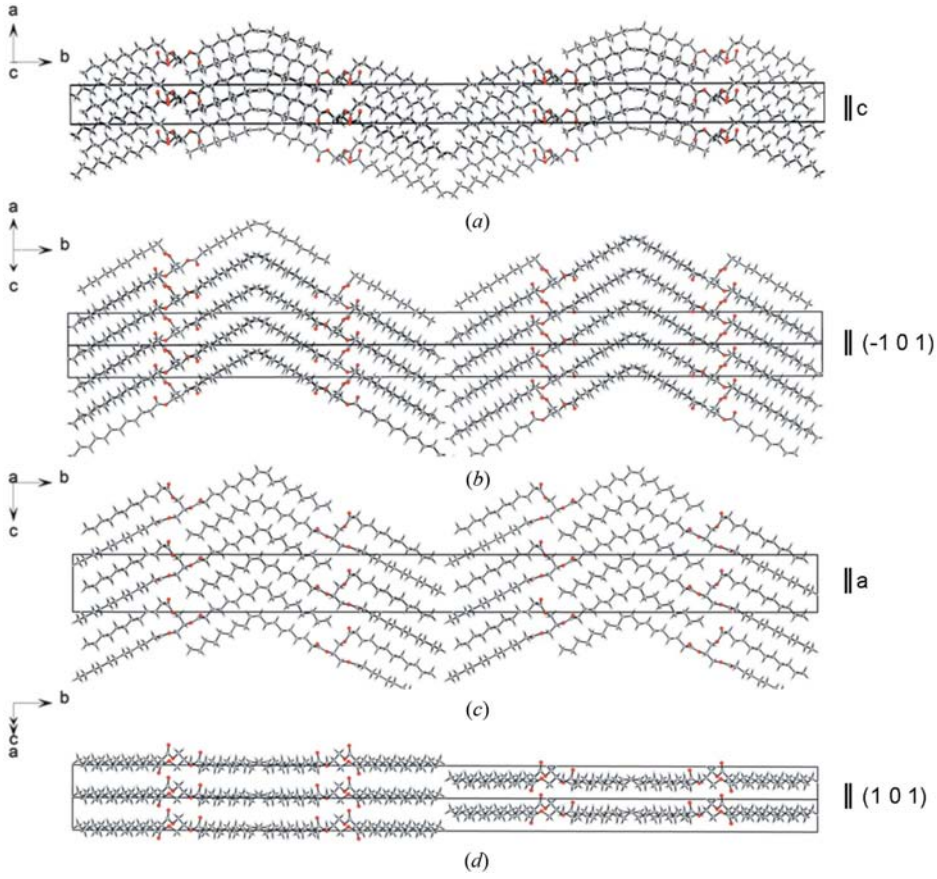

Figure 11
Parallel chain packing views of β_2-3 LaOLa rotating the structure around the *b* axis: (*a*) parallel to the *c* axis; (*b*) parallel to the ($\bar{1}$01) plane; (*c*) parallel to the *a* axis; (*d*) parallel to the (101) plane.

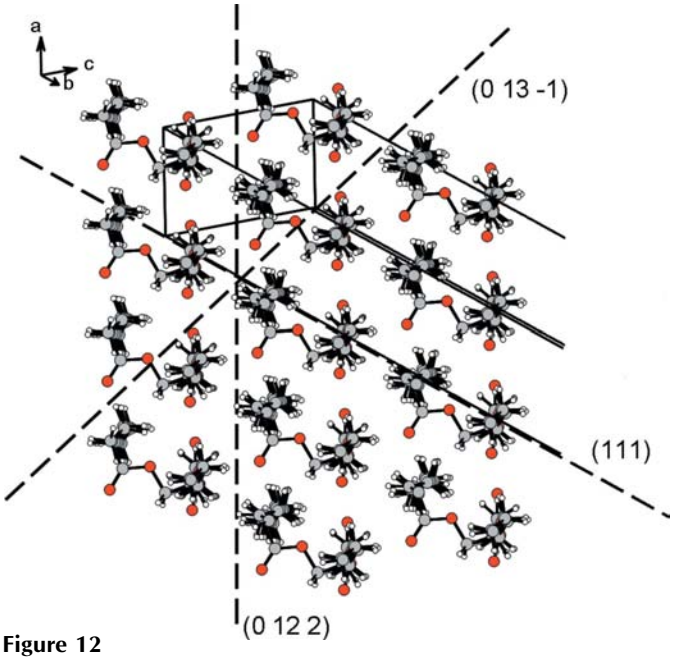

Figure 12
Crystal packing of β_2-3 LaOLa viewed with the chain direction perpendicular to the paper. Lattice planes of strong reflections have been marked, having *d* spacings of 4.58 (111), 3.91 (0,13,$\bar{1}$) and 3.69 Å (0,12,2), respectively. For clarity, the O2m chain has been omitted.

chains that give rise to the strong reflections in the fingerprint area (Fig. 11). Just like in the β'_1-2 packing, a view along the saturated chain direction shows the relation between strong fingerprint lines (Fig. 6, lower curve) and the chain packing (Fig. 12). The strong (111) diffraction maximum with a *d* spacing of 4.58 Å (19.5°2θ, Cu $K\alpha$) is characteristic for β-type Sat-O-Sat′ structures. The similarity of β_2-3 LaOLa to other β_2-3 Sat-O-Sat′ TAGs also suggests that a β_1-3 polymorph of LaOLa may exist, although no experimental evidence has been found yet that sustains this hypothesis.

Finally, a short comment is needed with respect to the synchrotron data of β_2-3. In retrospect, it turned out that the diffraction signal of the (020) long spacing had been shielded by the beam stop, but this does not seem to have had a decisive influence on getting the correct model. The height of the (020) diffraction maximum, as calculated from the final refined model, is 50% of the peak height of (040) and this agrees well with the intensity ratio that was observed for the same reflections at the β'-3 polymorph measured on the X'pert Pro MPD diffractometer.

3.5. Polymorphs and their transitions revisited

LaOLa has been shown to crystallize in three double chain-length polymorphs: α, β'_2-2 and β'_1-2, and two triple chain-length polymorphs: β'-3 and β_2-3. The existence of a β_1-3 polymorph, as found for related TAGs (van Mechelen *et al.*, 2006*b*) was not confirmed. A comparison of the crystal structures of the three polymorphs (β'_1-2, β'-3 and β_2-3) that have been solved from high-resolution XRPD data provides an explanation for the slow β'_1-2 $\rightarrow$ β_2-3 phase transition. The structure of β_2-3 LaOLa is similar to that of related β_2-3 Sat-O-Sat TAGs (van Mechelen *et al.*, 2006*b*) in which two saturated chains are packed parallel. However, both the β' structures have an unexpected molecular conformation in which a saturated chain (S3m) is parallel to part of the oleic chain (Figs. 3, 7 and 10). To achieve the β'_1-2 $\rightarrow$ β_2-3 transition, the S3m chain has to rotate 180° around the S3g chain and the

double chain-length packing has to be changed in a triple chain-length packing. This major conformational change explains the slow transition and makes a solid-state conversion unlikely.

With respect to the β'-3 $\rightarrow$ β'_1-2 phase transition, it has only been observed that the transition takes place if β'_1-2 seeds are present in a β'-3 melt. The transition of a pure β'-3 melt to the higher melting β'_1-2 has not yet been observed.

The authors wish to thank Unilever Research Vlaardingen for providing the pure LaOLa. The authors acknowledge the ESRF (Grenoble, France) for providing the facilities to perform the synchrotron diffraction experiments and they thank E. Dooryhee and A. Fitch of beamline BM16 for their valuable help during the experimental sessions. The authors also thank A. van Langevelde, W. Molleman, R.B. Helmholdt and E. Dova for their help in collecting data at BM16. Dr V. Favre-Nicolin is gratefully acknowledged to implement requested modifications in FOX. The investigations have been supported by the Netherlands Foundation for Chemical Research (NWO/CW) with financial aid from the Netherlands Technology Foundation (STW) (projects 790.35.405 and 790.35.616). The members of the User Committees of these projects are thanked for stimulating discussions and continuous interest.

References

Allen, F. H. (2002). *Acta Cryst.* B**58**, 380–388.
Arishima, T., Sagi, N., Mori, H. & Sato, K. (1991). *J. Am. Oil Chem. Soc.* **68**, 710–715.
Beckett, S. T. (1999). Editor. *Industrial Chocolate Manufacture and Use.* Oxford: Blackwell Science.
Collaborative Computational Project, Number 14 (1994). http://www.ccp14.ac.uk/solution/indexing/.
Favre-Nicolin, V. & Černý, R. (2002). *J. Appl. Cryst.* **35**, 734–743.
Jong, S. de, van Soest, T. C. & van Schaick, M. A. (1991). *J. Am. Oil Chem. Soc.* **68**, 371–378.
Kellens, M., Meeussen, W. & Reynaers, H. (1990). *Chem. Phys. Lipids*, **55**, 163–178.
Larson, A. C. & Von Dreele, R. B. (1987). *GSAS*. Report No. LAUR-86–748. Los Alamos National Laboratory, New Mexico, USA.
Larsson, K. (1972). *Fette Seifen Anstrichm.* **74**, 136–142.
Le Bail, A. (2004). *Powder Diffr.* **19**, 249–254.
Mechelen, J. B. van, Peschar, R. & Schenk, H. (2006*a*). *Acta Cryst.* B**62**, 1121–1130.
Mechelen, J. B. van, Peschar, R. & Schenk, H. (2006*b*). *Acta Cryst.* B**62**, 1131–1138.
Mechelen, J. B. van, Peschar, R. & Schenk, H. (2008*a*). *Acta Cryst.* B**64**, 240–248.
Mechelen, J. B. van, Peschar, R. & Schenk, H. (2008*b*). *Acta Cryst.* B**64**, 249–259.
Miura, S., Ogawa, A. & Konishi, H. (1999). *J. Am. Oil Chem. Soc.* **76**, 927–931.
Osborn, H. T. & Akoh, C. C. (2002). *Comput. Rev. Food Sci. Food Safety*, **3**, 93–103.
Peschar, R., Etz, A., Jansen, J. & Schenk, H. (2002). *Structure Determination from Powder Diffraction Data*, edited by W. I. F. David, K. Shankland, L. B. McCusker & Ch. Baerlocher, ch. 10. Oxford University Press.
Sato, K. (1996). *Adv. Appl. Lipid Res.* **2**, 213–268.
Sato, K., Arishima, T., Wang, Z. H., Ojima, K., Sagi, N. & Mori, H. (1989). *J. Am. Oil Chem. Soc.* **66**, 664–674.
Sato, K. & Ueno, S. (2001). *Crystallization Processes in Fats and Lipid Systems*, edited by N. Garti & K. Sato, ch 5. New York: Marcel Dekker.
Watanabe, A., Tashima, I., Matsuzaki, N., Kurashige, J. & Sato, K. (1992). *J. Am. Oil Chem. Soc.* **69**, 1077–1080.
Xu, X. B. (2000). *Eur. J. Lipid Sci. Technol.* **102,** 287–303.